Chemically-defined camelid antibody bioconjugate for the magnetic resonance imaging of Alzheimer's disease

Matthias Vandesquille, Tengfei Li, Chrystelle Po, Christelle Ganneau, Pascal Lenormand, Clémence Dudeffant, Christian Czech, Fiona Grueninger, Charles Duyckaerts, Benoit Delatour, et al.

Report

Chemically-defined camelid antibody bioconjugate for the magnetic resonance imaging of Alzheimer's disease

Matthias Vandesquille,[1,2,4,*] Tengfei Li,[3,5,6,*] Chrystelle Po,[1,2,4,**] Christelle Ganneau,[1,2] Pascal Lenormand,[3] Clémence Dudeffant,[5] Christian Czech,[7] Fiona Grueninger,[7] Charles Duyckaerts,[5] Benoît Delatour,[5] Marc Dhenain,[4,*] Pierre Lafaye,[3,*] Sylvie Bay[1,2]

[1]Institut Pasteur, Unité de Chimie des Biomolécules, 75724 Paris Cedex 15, France

[2]CNRS UMR 3523, 75724 Paris Cedex 15, France

[3]Institut Pasteur, Plateforme d'Ingénierie des Anticorps, 75724 Paris Cedex 15, France

[4]French Alternative Energies and Atomic Energy Commission, Institute of Biomedical Imaging, Molecular Imaging Research Center, 92260 Fontenay-aux-Roses, France

[5]Sorbonne Universités, UPMC Univ. Paris 06 UMR S 1127, and Inserm, U 1127, and CNRS UMR 7225, and ICM, F-75013, Paris, France

[6]Université Paris Diderot-Paris 7, France

[7]F. Hoffmann-La Roche AG, Pharmaceutical Research and Early Development, NORD DTA, Roche Innovation Center Basel, CH-4070 Basel, Switzerland

[$]Correspondence to: Sylvie Bay; E-mail: sylvie.bay@pasteur.fr, Address: Institut Pasteur, 28 rue du Dr Roux - 75724 Paris Cedex 15, France.

[**]Present address: ICube - Institut de Physique Biologique - Faculté de Médecine, 4 rue Kirschleger, 67085 Strasbourg Cedex, France.

[*]These authors equally contributed to this work.

The authors declare no competing financial interest. C. Czech and F. Grueninger are employees of F. Hoffmann-La Roche.

ABSTRACT

Today, molecular imaging of neurodegenerative diseases is mainly based on small molecule probes. Alternatively, antibodies are versatile tools that may be developed as new imaging agents. Indeed, they can be readily obtained to specifically target any antigen of interest and their scaffold can be functionalized. One of the critical issues involved in translating antibody-based probes to the clinic is the design and

synthesis of perfectly-defined conjugates. Camelid single-domain antibody-fragments (VHHs) are very small and stable antibodies that are able to diffuse in tissues and potentially cross the blood brain barrier (BBB). Here, we selected a VHH (R3VQ) specifically targeting one of the main lesions of Alzheimer's disease (AD), namely the amyloid-beta (Aβ) deposits. It was used as a scaffold for the design of imaging probes for magnetic resonance imaging (MRI) and labeled with the contrastophore gadolinium using either a random or site-specific approach. In contrast to the random strategy, the site-specific conjugation to a single reduced cysteine in the *C*-terminal part of the R3VQ generates a well-defined bioconjugate in a high yield process. This new imaging probe is able to cross the BBB and label Aβ deposits after intravenous injection. Also, it displays improved r1 and r2 relaxivities, up to 30 times higher than a widely used clinical contrast agent, and it allows MRI detection of amyloid deposits in *post mortem* brain tissue of a mouse model of AD. The ability to produce chemically-defined VHH conjugates that cross the BBB opens the way for future development of tailored imaging probes targeting intracerebral antigens.

KEYWORDS

single-domain antibody, chemically-defined imaging probe, site-specific conjugation, Alzheimer's disease diagnosis, amyloid deposits, Magnetic Resonance Imaging.

ABBREVIATIONS

Aβ amyloid-beta

AD Alzheimer's disease

BBB blood-brain barrier

CDR complementarity determining region

DOTA 1,4,7,10-tetraazacyclododecane-*N*,*N*,*N*,*N*-tetraacetic acid

ELISA enzyme-linked immunosorbent assay

Gd gadolinium

IC_{50} median inhibition concentration

IHC immunohistochemistry

M_r relative molecular mass

MRI magnetic resonance imaging

MS mass spectrometry

NHS *N*-hydroxysuccinimide

SDS-PAGE sodium dodecyl sulfate polyacrylamide gel electrophoresis

SEC size-exclusion chromatography

TCEP tris(2-carboxyethyl)phosphine

VHH variable domain of camelid heavy-chain antibodies.

INTRODUCTION

Molecular imaging based on the design of specific probes is a key method for diagnosis of human diseases. Antibodies are versatile tools for developing future generation of molecular imaging agents. Specific antibodies can be readily obtained to target a wide range of antigens and they can be labeled with various imaging agents, mostly through the primary amines of lysines or the thiol functions of cysteines.[1] However, as these functions are distributed throughout the antibody structure, their derivatization can lead to modification of the antibody properties, notably the antigen recognition by steric hindrance of the complementary-determining regions (CDRs). Moreover, this random conjugation is poorly reproducible and generates non-homogeneous batches of conjugates, thus severely limiting potential clinical development. The generation of well-defined bioconjugates is emerging as a critical issue in molecular imaging research.

To this end, several elegant strategies based on site-specific coupling have been designed to obtain conjugates with preserved biological activity.[2-7] These methods typically introduce far from the binding site a functional group that specifically reacts with the reagent of interest. For example, the use of non-native amino acids with ketones or azides allows strict control over the site and the stoichiometry of the reaction.[8,9] Although successful, these methods suffer from several limitations in terms of feasibility,

scalability, and efficacy. Another common and straightforward strategy consists of introducing a cysteine that can react with various thiol-specific coupling reagents. Along this line, cysteines have been successfully derivatized after being inserted within the sequence[10] or at the *C*-terminal region of different types of antibodies.[11-17] This technique allows the stoichiometric ligation of the reagent on a single site, assuming that no other reduced cysteine is available, and leads to conjugates with unmodified (or nearly unmodified) properties compared to the original antibody.[10-12]

One class of promising antibodies for *in vivo* imaging is camelid single-domain antibody-fragments (VHHs),[18,19] also called nanobodies. VHHs offer numerous advantages for molecular imaging diagnosis. They are very stable, highly specific for the target antigen, and they bind epitopes not recognized by conventional antibodies.[20-22] Their small size (hydrodynamic radius of 2-2.5 nm for a molecular weight around 15 KDa) enables them to diffuse in tissue more efficiently than conventional antibodies.[23,24] VHHs have a limited immunogenicity[25] due to their short half-life and to their high homology with human VH sequences.[26] Moreover they can be easily humanized for clinical studies without loss of their properties.[27] Recent studies have demonstrated that some VHHs are able to cross the blood-brain barrier (BBB).[28-31] Because they lack the Fc fragment, they cannot be exported outside the brain via the FcɣR mediated efflux system present at the BBB.[32] Thus, VHHs represent promising scaffolds for the development of imaging nanoprobes, particularly for intracerebral biomarkers.

Alzheimer's disease (AD) is the most common form of neurodegenerative disease. In the last decade, several molecular imaging probes targeting the two main neuropathological hallmarks of this disease, amyloid deposits and neurofibrillary tangles, have been engineered.[33-37] These agents are based on small radioactive molecules developed for positron emission tomography (PET).[38,39] As an alternative to PET, several magnetic resonance imaging (MRI) contrast agents have been developed for amyloid deposits detection.[40-44] However, these compounds do not penetrate in the brain spontaneously and require the use of invasive techniques (*e.g.,* BBB transient opening using hyperosmotic agents or ultrasound-associated microbubble injections) to reach their target.

Hence, our objective was to obtain a VHH antibody-based probe that crosses the BBB and can be used for MRI of amyloid deposits. One of the key issues for the development of such an agent is the synthesis of chemically-defined conjugates that can provide in a perfectly reproducible manner compounds that may be translated to the clinic. In this context, we selected a VHH antibody (R3VQ) specifically targeting amyloid deposits and we designed gadolinium (Gd)-VHH conjugate MRI probes using either random or site-specific approach (ligation through lysine or cysteine residues, respectively). In contrast to the random coupling, the site-specific thio-addition to a reduced cysteine of R3VQ resulted in a chemically-defined imaging agent. This bioconjugate crossed the BBB and reached its intracerebral target after intravenous injection in mice. Finally, it had high MR relaxivities and was able to efficiently detect amyloid deposits by *in vitro* MRI in

mice. Overall, our results describe the synthesis of a high quality VHH-based contrast agent that is functionally intact and crosses the BBB, thus opening future developments of tailored imaging probes targeting intracerebral antigens.

RESULTS

Selection, design and production of anti-amyloid-beta VHHs

To design an imaging agent for the diagnosis of AD by MRI, the first step was to obtain a probe specifically targeting amyloid deposits and containing site(s) for ligation to an MRI contrast agent.

After immunization with a fibrillar synthetic amyloid-beta (Aβ)42 peptide, a specific VHH called R3VQ was selected by phage display (Figure S1A). Soluble R3VQ was then expressed in *E. coli* with a *C*-terminal 6-Histidine tag to allow its purification and immunodetection (Figure S1B).[47] This VHH, referred as R3VQ-NH_2 **1**, was shown to recognize amyloid deposits by immunohistochemistry (IHC) on brain slices from a mouse model of AD (PS2APP[48]) (Figure S2). This construct was used for the random conjugation approach involving the formation of amide bond between the primary amines (-NH_2) contained in the sequence (four lysine ε-amines and one *N*-terminal α-amine; all located out of the CDRs) with a *N*-hydroxysuccinimide (NHS) ester compound.

A further R3VQ construct was prepared for the site-specific conjugation. Because this reaction involved a thio-addition with a maleimide reagent, it was necessary to generate R3VQ with a sterically accessible cysteine residue. We thus designed R3VQ-SH **3** containing the original sequence (presence of two canonical cysteines embedded in the sequence near the CDRs) with an additional cysteine residue in the *C*-terminal part. A thrombin cleavage site was introduced between the VHH sequence and the *N*-terminal tag to allow its removal if necessary for further *in vivo* developments (Figure S1C).

After purification, the two VHHs **1** and **3** (16-20 mg/L of culture) were analyzed by quantitative amino acid analysis (AAA), sodium dodecyl sulfate-polyacrylamide gel electrophoresis (SDS-PAGE) (Figure S3), and mass spectrometry (MS) (Figure 1A and B). These methods confirmed the identity and high level of purity of the two constructs.

Chemical conjugation of anti-Aβ VHHs to the contrast agent

Two different strategies were then implemented to link the VHHs with 1,4,7,10-tetraazacyclododecane-*N*,*N*,*N*,*N*-tetraacetic acid (DOTA)/Gd: the random and the site-specific approaches based on the derivatization of R3VQ-NH_2 **1** (Scheme 1A), and R3VQ-SH **3** (Scheme 1B), respectively.

Random conjugation

This approach involved the conjugation of the DOTA-NHS ester on the primary amines of R3VQ-NH_2 **1**, followed by the chelation of Gd with the DOTA (Scheme 1A). First, a buffer exchange was required after the affinity chromatography to remove the imidazole contained in the elution buffer of **1**, as it will

otherwise promote the hydrolysis of the active ester.[1,49] The conjugation was then performed with two conditions leading to different degrees of derivatization. The first condition was implemented with the reaction of 4 fold-molar excess of DOTA-NHS per reactive amino group and led to a polydisperse mixture with 0-2 DOTA per protein. Forced conditions, with higher excess of DOTA-NHS added portionwise, resulted in a mixture with 3-5 DOTA per protein. Following buffer exchange, the chelation of the Gd was performed at pH 5. After removal of the excess Gd reagent and buffer exchange, two mixtures of R3VQ-N-$(DOTA/Gd)_n$ were obtained with different levels of conjugation. The average number of DOTA/Gd (n) was between 0 and 2 (**2a,** Figure 1C) or 3 and 5 (**2b,** Figure S4) as determined by MS analyses (respective yield 67% and 74%). Interestingly for **2b**, the heterogeneity was observed at both DOTA and Gd levels since complete chelation could not be achieved despite extra addition of Gd reagent and extended reaction time.

Site-specific conjugation

This approach involved the conjugation of a maleimide-$(DOTA/Gd)_3$ **4** to the extra cysteine of R3VQ-SH **3** (Scheme 1B). The Gd trimer was chosen to optimize the relaxometric parameters, essential for the detection sensitivity. The synthesis of **4** was accomplished on solid-phase using Fmoc chemistry, DOTA lysine building blocks and (1H-9-azabenzotriazole-1-yl)-1,1,3,3-tetramethyluronium hexafluorophosphate (HATU) / diisopropylethylamine (DIEA) as the coupling reagent (Scheme 2). Glycine residues were introduced as spacers between each DOTA motif. After cleavage from the resin, the DOTA-peptide intermediate was chelated with Gd at pH 5. The purification on reverse phase afforded **4** with an overall yield of 64%, a purity greater than 95% (Figure S5A), and the expected molecular weight together with the typical isotopic distribution (Figure S5B).

For the thio-addition with the maleimide compound **4**, it was essential to check the redox state of the two canonical cysteines as well as of the extra cysteine of the VHH sequence. To this end, MS analyses were performed on R3VQ-SH **3** after reduction/alkylation experiments, with or without denaturation (Figure 1E). The alkylation of **3** in the presence of iodoacetamide after reduction by tris(2-carboxyethyl)phosphine (TCEP) led to a shift of 57 Da of the observed M_r, meaning that only one cysteine was alkylated. Notably, mild reduction conditions allowed to reduce the intermolecular dimer of R3VQ-SH **3** (progressively formed upon storage), and to recover the single reduced cysteine, while keeping the disulfide bridge intact (see Figure S6 for HPLC, size-exclusion chromatography (SEC) and MS analyses). By contrast, strong denaturation with RAPIGEST at 55 °C before reduction allowed disruption of the internal disulfide bond and led to alkylation of the three cysteines by iodoacetamide in the same conditions, as showed by a shift of 171 Da of the major MS peak. The minor di-alkylated derivative was also observed (+114 Da). Interestingly, complete alkylation could not be achieved either with longer reaction time or stronger denaturation conditions, in agreement with previous data showing the high stability of VHHs.[50,51]

Altogether, these results confirmed the high stability of the internal disulfide bond and the accessibility of a unique reduced cysteine for site-specific conjugation after a mild reduction.

Conjugation of compound **4** with R3VQ-SH **3** was first realized after a buffer exchange in phosphate-buffered saline (PBS)/NaCl resulting in the conjugate **5** with a yield of 70%. Side-reaction between maleimide groups and imidazole (contained in the initial buffer) was expected as previously reported by several groups showing the histidine side-chain alkylation.[52,53] Nonetheless, further investigation revealed that **4** could be directly conjugated to **3** in the affinity column elution buffer, with limited excess of the maleimide reagent and despite a large molar excess of imidazole. After a final diafiltration to remove the imidazole and excess reagent, the chemically-defined conjugate R3VQ-S-(DOTA/Gd)$_3$ **5** was obtained with a yield of 83% and a high quality, as demonstrated by MS (Figure 1D), SDS-PAGE (Figure S3), RP-HPLC (Figure S6A) and SEC (Figure S6B) analyses.

Functional characterization of the conjugates

Binding to the target in vitro and in vivo

To assess the functional properties of the compounds, IHC was performed on brain tissue sections from PS2APP mice that have extensive Aβ deposition[48] and wild-type amyloid-free mice. Similar immunostaining of amyloid plaques was always detected by an anti-His-tag secondary antibody when brain sections from PS2APP mice were incubated with different R3VQ-based compounds (Figure 2 and S2). As control experiments, anti-His-tag immunostaining was evaluated on brain sections from PS2APP mice that were not incubated with R3VQ-based compounds. A slight non-specific labeling of some cells could be detected, but definitely not associated with any amyloid plaques (Figure S7A). Brain sections from PS2APP mice were similarly evaluated after incubation with a non-relevant VHH targeting pTau epitopes,[47] a major constituent of neurofibrillary tangles that are absent in these mice. No staining was observed, whether the irrelevant VHH was conjugated or not (Figure S7B and C). Finally, brain tissues from wild-type amyloid-free mice were incubated with **5** (Figure S7D) or with a non-relevant VHH targeting pTau epitopes (Figure S7E and F). Anti-His-tag immunostaining also did not show any specific staining. These results confirmed the ability of R3VQ compounds to specifically recognize Aβ deposits in the brain of PS2APP mice.

To evaluate the binding properties of the VHHs and their conjugates in more detail, we investigated their ability to bind Aβ40 peptide by enzyme-linked immunosorbent assay *(*ELISA) (Table 1). Aβ40 was preferred to Aβ42 because 1) both peptides are similarly recognized by R3VQ[47] and 2) the higher propensity of Aβ42 to aggregate led to inconsistent results.[22,54] Comparison of the median inhibition concentration (IC_{50}) of the two VHHs **1** and **3** showed no significant difference (16 *vs* 18 nM, respectively) indicating that the addition of a cysteine did not affect the affinity of the VHH. By contrast, the

corresponding conjugates showed a marked difference. The random conjugation induced an increase of the IC_{50} related to the number of DOTA/Gd linked to the VHH **(**24 nM for **2a** and 50 nM for **2b**), whereas the site-specific method left the IC_{50} value unaffected (19 nM for **5**).

Considering the drawbacks of the random approach, further investigation was focused on the well-defined compound **5**. We assessed the capacity of **5** to cross the BBB *in vivo*, a prerequisite to reach its intracerebral target (*i.e.,* amyloid deposits) and to allow future *in vivo* imaging assays. PS2APP mice were injected in the tail vein with PBS or **5**. Mice were sacrificed after 4 hours, and IHC were realized with an anti-His-tag secondary antibody. By contrast to the mice injected with PBS, a specific labeling of amyloid deposits was detected in those injected with the conjugate **5** (Figure 3). Also, comparison of anti-His-tag immunostaining of PS2APP brain tissue obtained after intravenous administration of **5** or after direct incubation of an entire brain hemisphere with **5** showed similar detection of amyloid deposits in both conditions (Figure S8). These results demonstrated the ability of the R3VQ-S-$(DOTA/Gd)_3$ **5** to cross the BBB, to diffuse in the brain parenchyma and to target Aß lesions after *in vivo* injection.

MR relaxometric parameters of R3VQ-S-$(DOTA/Gd)_3$ 5

The main determinants of the contrast in an MR image are the proton relaxation times T1 and T2. MR contrast agents modulate these relaxation parameters to improve the contrast on the images, and contrast agents are characterized by their relaxometric parameters r1 and r2, which refer to the amount of increase in 1/T1 and 1/T2, respectively, per millimolar of agent.[55] We thus determined the T1-relaxivity (*i.e.,* r1) and T2-relaxivity (*i.e.,* r2) of the reagent **4** and the conjugate **5** at 1.4, 7 and 11.7 Tesla, and compared the results to those obtained with a widely used clinical contrast agent (*i.e.,* DOTA/Gd, DOTAREM). Results are presented in Figure 4 (for detailed results see Figure S9).

The r1 and r2 relaxivities of **4** were 1.6 to 2.7 times higher than those of DOTA/Gd in H_2O. Analysis of the r1 and r2 relaxivities of the final conjugate **5** showed values 3.7 to 4.6 times higher than relaxivities of **4**, and 6.8 to 10.1 times higher than those of DOTA/Gd.

MRI visualization of amyloid deposits following in vitro incubation with R3VQ-S-$(DOTA/Gd)_3$ 5

Finally, we investigated the efficiency of the imaging agent **5** to detect amyloid deposits by MRI. Cerebral hemispheres of wild-type (amyloid-free) mice were incubated with **5** and hemispheres from PS2APP were incubated with **5** or PBS overnight. Then, hemispheres were rinsed for 48 hours and imaged with a 25 µm isotropic resolution (field of view: 12.8x12.8x6.4 mm^3) on an 11.7 Tesla spectrometer (Figure 5A, left frames). The density of hypointense spots detected on MR images was increased sevenfold in PS2APP hemispheres incubated with **5** compared to PS2APP hemispheres incubated in PBS (50.97 ± 8.53 *vs* 7.32 ± 0.11 spots/mm^2), and by 33 times compared with hemispheres from wild-type mice incubated with **5** (50.97 ± 8.53 *vs* 1.53 ± 0.04 spots/mm^2) (Figure 6). Following MRI, brain tissues were processed by IHC with the reference anti-amyloid antibody 4G8 and an anti-His-tag antibody. The presence of amyloid deposits in

PS2APP brains was indeed confirmed whereas no deposits were observed in wild-type mice (Figure 5A, middle frames). To validate the specificity of the MRI labeling with **5** in PS2APP, MR images were registered with 4G8 (Figure 5B, middle frame) and anti-His-tag (Figure 5B, right frame) sections. The numerous hypointense spots observed on MR images were co-localized with amyloid deposits detected by 4G8 IHC, and with the conjugate **5** labeled by anti-His-tag (Figure 5B, red arrows). PS2APP brains incubated in PBS did not show hypointense spots on MRI and, on histological sections, their amyloid plaques were not labelled by anti-His-tag (Fig. 5A, PS2APP/PBS frames). Hemispheres of wild-type mice devoid of amyloid deposits incubated with **5** did not display any hypointense spots on MRI nor any spots labelled with anti-His-tag on histological sections (Fig. 5A, Wild-type/**5** frames). Taken together, these results demonstrated a strong increase of amyloid plaque detection in MR images of PS2APP brains following incubation with **5**.

DISCUSSION

High-yield chemoselective conjugation provides a chemically-defined VHH-based imaging probe

One of the key issues for the development of antibody-based probes is the synthesis of perfectly defined conjugates, which allows stringent quality control. We designed new imaging probes by linking an Aβ-specific VHH (R3VQ) to the MR contrastophore Gd through a DOTA chelate following two strategies: the random conjugation to the primary amines of the VHH and the site-specific conjugation to a cysteine introduced in the *C*-terminal part of the VHH.

We found that the random approach produced variable batches, which are difficult to reproduce and may lead to unreliable results due to the variable amount of DOTA/Gd. For example, the obtained unlabeled and over-labeled VHHs can result in a saturation effect, in a modification of the VHH properties for its target, or in a significant impact on their pharmacokinetics, as recently shown with a near-infrared fluorescent VHH.[56] In our case, the functional properties of the conjugate mixtures were indeed affected compared to the starting VHH, with a significant decrease of the Aβ recognition when one to two DOTA/Gd are attached. This effect could be due to steric hindrance in the vicinity of the antigen recognition site, which increased when more amino groups are derivatized.[57]

In contrast, the site-specific conjugation led to a well-defined homogeneous compound labeled uniquely in its *C*-terminal part with a defined amount of contrast agent (*i.e.,* three Gd per VHH). This represents a critical advantage for consistent studies and for translation to clinic. Indeed, antibody-based drugs have attained tremendous success in the past decade, and several reports have highlighted the importance of their quality control.[58,59] It is worth noting that we implemented the site-specific conjugation in an easy and a high-yield optimized process. To our knowledge, one-pot thio-addition of maleimide compounds to a

protein directly eluted from the affinity purification column has never been described before. This novel strategy simplifies the process and improves the overall yield of the resulting conjugate.

Our synthetic approach is fully convergent since the preformed Gd building block is tethered to the VHH at the last step. Taking advantage of suitably functionalized synthons, it can therefore facilitate the generation of a variety of conjugates, while enabling the fine tuning of their composition (*e.g.,* stoichiometry of the contrastophore, nature of the spacer). The chemical structures can be even more diversified by using other VHH of interest as the scaffold, as recently shown by our group with an anti-Tau VHH targeting neurofibrillary tangles.[47] The conjugates and their modular construction can be readily designed according to their downstream application.

R3VQ-S-(DOTA/Gd)$_3$ imaging probe crosses the BBB and binds to amyloid deposits *in vivo*

We then focused on the well-defined R3VQ-S-(DOTA/Gd)$_3$ conjugate and evaluated its functionality. Development of molecular imaging probes for intracerebral targets remains challenging. Antibodies are valuable tools for developing such specific probes, but their penetration in the central nervous system is prevented by the BBB. In the case of AD, a few antibody-derived small proteins (*i.e.,* VHHs and affibodies) have been proposed to target Aβ peptides. Most of them recognize only the dimeric or oligomeric forms of the peptide and thus are mainly described to block amyloid deposits formation. [22,28,60-64]

To our knowledge, only a few VHHs directed against human parenchymal amyloid deposits have been reported,[30,31] with one described as able to efficiently cross the BBB *in vitro.*[31]

Although several studies have also shown that several VHHs are able to penetrate into the brain *in vivo,*[28,29,47] BBB crossing by VHH remains highly variable.[30,65] Here, we show that R3VQ-S-(DOTA/Gd)$_3$ binds the Aβ peptide with high specificity and sensitivity and labels amyloid deposits on brain section of a mouse model of amyloidosis. Furthermore, we demonstrated its ability to cross the BBB and to label amyloid deposits after intravenous injection in mice. This result is consistent with our recent publication showing, by *in vivo* two-photon imaging and *ex vivo* IHC, that R3VQ conjugated to a fluorescent label does cross the BBB.[47] Knowing that the DOTAREM (*i.e.,* the monomer building block of compound **4**) does not cross the BBB by itself,[40] all our results suggest that the R3VQ allows the contrast agent of interest to penetrate at least partially into the brain. Hence, contrary to previously described Aβ-targeting VHH, affibodies and conventional antibody-based strategies, R3VQ crosses the BBB on its own, rapidly diffuses into the brain and reaches its intracerebral target *in vivo*. It remains that the BBB penetration by VHH cannot be generalized, may arise from different mechanisms and surely depends on the considered VHH.

R3VQ-S-(DOTA/Gd)$_3$ contrast agent has high relaxivities and detects amyloid deposits in brain tissue

A contrast agent is characterized by relaxivity parameters r1 and r2 that reflect its potential to actually modify contrast on MR images. Interestingly, the r1 and r2 relaxivities of R3VQ-S-(DOTA/Gd)$_3$ **5** reached values up to 5 times higher than those of the non-conjugated synthon **4** and 10 times higher than those of a clinically used contrast agent (*i.e.,* DOTAREM). Notably, as relaxivity is expressed relative to the Gd concentration, and considering that each VHH is linked to three Gd, the overall relaxometry of R3VQ-S-(DOTA/Gd)$_3$ **5** was up to 30 times higher than that of DOTAREM. Two hypotheses can explain this dramatic increase in r1 and r2: 1) an increase in the size and rigidity of the contrast agent resulting from the conjugation, which probably led to the reduced rotational correlation time and thus an increased relaxivity; and 2) the capturing of water molecules within the VHH vicinity, which led to the increased number of outer sphere-coordinated water molecules.

In our last experiment, we evaluated the potential of R3VQ-S-(DOTA/Gd)$_3$ **5** to reveal amyloid deposits by MRI. Whole brains from transgenic mouse model of amyloidosis (PS2APP) were incubated with the imaging probe or PBS, and were then imaged by MRI at 11.7 Tesla with a high isotropic resolution of 25 µm. Control images of PS2APP brains incubated in PBS showed a small number of hypointense lesions, probably due to blood vessels and amyloid deposits containing iron as previously described.[66-68] MR images of brains incubated with R3VQ-S-(DOTA/Gd)$_3$ **5** demonstrated a significant increase in the number of detected hypointense spots, 7 times higher than in PS2APP brains incubated with PBS. Registration of MR images with 4G8-stained histological sections confirmed that the spots corresponded to amyloid deposits. A second registration with histological sections stained with an anti-His-tag antibody confirmed that the MR hypointense spots corresponded to R3VQ-S-(DOTA/Gd)$_3$ **5** accumulation. Some mismatch between hypointense spots, anti-His-tag and 4G8-positive labels could be explained by methodological discrepancies due to limitations in the precision of co-registration resulting from the different thickness of MRI and IHC sections (25 µm versus 5 µm, respectively) and from tissue deformation associated to different histological steps (fixation, paraffin embedding, brain cutting). Moreover, 4G8 antibody was incubated directly on slices, whereas the R3VQ-S-(DOTA/Gd)$_3$ **5** was incubated on the whole brains. Hence, diffusion or concentration differences could explain that fewer deposits or fainter staining were visible following anti-His-tag IHC. Nevertheless, the majority of the amyloid deposits labeled by the anti-His-tag antibody were visible on the MR images. Finally, images acquired on wild-type brains incubated with the imaging probe did not show any contrast modification, thus confirming the absence of unspecific labeling on MR images. This experiment thus shows that the imaging agent **5** is able to readily diffuse in tissue, which is consistent with previous reports,[23,24] and that it specifically modifies the contrast of amyloid deposits on MR images, allowing their visualization and thus opening new perspectives for *in vivo* imaging.

Developing sensitive contrast agents for MRI detection of amyloid deposits is very challenging. Further development of R3VQ-Gd-based reagent for *in vivo* imaging applications still relies on several

optimizations. New synthon design is possible to further improve the relaxometric properties of the conjugate, in particular by increasing its DOTA/Gd content, or by constraining its structure *i.e.,* reducing the rotational correlation time of the contrast agent. One can also improve its ability to cross the BBB, for example by modulating its basic isoelectric point.[29] After its penetration in the brain, the increase in the local concentration of the VHH-based probe around amyloid deposits, due to its affinity for the plaques, is also a critical parameter that could be further improved. Finally, toxicity and pharmacokinetic properties should be taken into account. Considering the stability of the chelate, along with the reported short half-life (around 12 min), the free gadolinium toxicity should not be an issue.[69-72] The pharmacokinetic profile of R3VQ-S-(DOTA/Gd)$_3$ **5** will allow optimization of the injected dose and the time-frame according to its clearance.

In conclusion, our study describes the design of a chemically-defined bioconjugate combining the properties of 1) an antigen-specific VHH that crossed the BBB, and 2) a Gd contrast agent. We highlight the advantages of the site-specific labeling that provides, in an easy two-step process, a high quality imaging probe along with intact functional properties. All these parameters are essential when considering the translation to clinic, which requires highly specific and well-defined probes. Our imaging agent spontaneously crossed the BBB, reached its intracerebral target *in vivo*, and also displayed high relaxivities allowing the detection of amyloid deposits *in vitro* by MRI. The efficacy, the versatility and the robustness of our synthetic strategy, together with the unique properties of site-specific engineered VHHs opens the way for future development of tailored VHH-based imaging probes targeting intracerebral antigens.

MATERIALS AND METHODS

Production of R3VQ, R3VQ-NH$_2$ 1 and R3VQ-SH 3

The three proteins were prepared as previously described.[47] Both G$_3$S spacer and *C*-terminal dipeptide SA improved the expression of the VHH **3**. The VHHs **1** and **3** were purified by immobilized metal affinity chromatography (HITRAP charged with Ni^{2+}). After extensive washings with PBS containing 300 mM NaCl (PBS/NaCl) and 0.1% Triton X114 (100 column volumes), and then PBS/NaCl (100 column volumes), they were eluted in PBS/NaCl buffer containing 500 mM imidazole (PBS/NaCl/imidazole). All VHHs reached high production yield (16-20 mg/L of culture) and low level of endotoxin (< 0.5 EU/mL, as measured by the Chromogenic Limulus Amebocyte Lysate assay following the manufacturer's instructions (Lonza)).

R3VQ-NH$_2$ **1**

AAA: Ala 15.8 (16), Arg 9.1 (9), Asp+Asn 13.4 (13), Glu+Gln 16.0 (15), Gly 13.4 (14), His 5.7 (7), Ile 3.1 (3), Leu 8.4 (8), Lys 4.1 (4), Phe 4 (4), Pro 6.1 (7), Ser 11.3 (13), Thr 10.0 (11), Tyr 4.8 (5), Val 11.1 (11).

MS: 15,752.0088 ($C_{681}H_{1053}N_{209}O_{216}S_4$ calcd 15,752.3949)

R3VQ-SH **3**

AAA: Ala 16.1 (16), Arg 10.2 (10), Asp+Asn 13.6 (13), Glu+Gln 11.9 (11), Gly 19.1 (20), His 6.0 (7), Ile 3.1 (3), Leu 8.5 (8), Lys 2.2 (2), Phe 4 (4), Pro 4.3 (4), Ser 15.5 (18), Thr 9.5 (10), Tyr 4.8 (5), Val 12.9 (12).

MS: 15,724.5859 ($C_{671}H_{1041}N_{213}O_{217}S_5$ calcd 15,724.2820).

Synthesis of R3VQ-N-(DOTA/Gd)$_n$ 2a and 2b

The R3VQ-NH_2 **1** eluted from the affinity column was dialyzed in PBS/NaCl. 1,4,7,10-tetraazacyclododecane-1,4,7,10-tetraacetic acid mono (*N*-hydroxysuccinimide ester) (DOTA-NHS) (274 µg, 4 eq. relative to amino group) dissolved in PBS/NaCl (120 µl) was added to **1** (480 µL, 0.6 mg/mL) and the solution was stirred at room temperature. Aliquots (10 µL) were withdrawn every 15 min, diluted with 100 mM Tris buffer pH 7.3 (90 µL) and analyzed by HPLC/MS to monitor the reaction progress. After 3 h, the solution was cooled to 4 °C and the buffer was exchanged to 0.4 M Na acetate buffer pH 5 by using VIVASPIN 500 centrifugal filter device (3,000 MWCO PES) (Sartorius). The resulting DOTA-VHH conjugate (480 µL) was added with $GdCl_3$ (149 µg, 45 eq. relative to average DOTA groups) in the same buffer (5 µL). The solution was stirred at room temperature for 2.5 h. The buffer was exchanged to PBS/NaCl at 4 °C with the same VIVASPIN device as above and the solution was concentrated to afford the R3VQ-N-(DOTA/Gd)$_{0\text{-}2}$ conjugate **2a** (105 µL, 1.48 mg/mL). The overall yield is 67%. The conjugate **2b** was obtained using the same protocol except that DOTA-NHS was added to **1** portionwise (0.5 eq every 45 min, total of 5.5 eq. relative to amino groups)**.** The solution was stirred at room temperature for 8 h. The overall yield is 74%.

R3VQ-N-(DOTA/Gd)$_{0\text{-}2}$ **2a**

AAA: Ala 16.0 (16), Arg 10.0 (9), Asp+Asn 12.8 (13), Glu+Gln 15.0 (15), Gly 13.8 (14), His 6.7 (7), Ile 3.0 (3), Leu 8.2 (8), Lys 4.5 (4), Phe 4 (4), Pro 8.5 (7), Ser 10.5 (13), Thr 10.1 (11), Tyr 4.8 (5), Val 11.1 (11).

MS: 16,293.1328 ((DOTA/Gd)$_1$: $C_{697}H_{1076}N_{213}O_{223}S_4Gd$ calcd 16,293.0421)

16,833.5586 ((DOTA/Gd)$_2$: $C_{713}H_{1099}N_{217}O_{230}S_4Gd_2$ calcd 16,833.6735)

Synthesis of R3VQ-S-(DOTA/Gd)$_3$ 5

To study the redox state of the VHH cysteines, R3VQ-SH **3** was submitted to a reduction (157 eq. of TCEP, 25 °C, 1 h, pH 8.2) followed by an alkylation (78 eq. of iodoacetamide, 25 °C, 1 h, pH 7.5) in an 0.1 M ammonium hydrogen carbonate buffer pH 8.2, with or without previous denaturation (RAPIGEST SF 0.1%, 55 °C, 1 h, pH 8.2, according to manufacturer's protocol).

The R3VQ-SH **3** eluted from the affinity column was dialyzed in PBS/NaCl. Due to the tendency of R3VQ-SH **3** to dimerize, a mild reduction step was introduced before the synthesis of **5** (5 eq. of TCEP, 30 min at 4 °C). **4** (1.35 mg, 3 eq. per VHH) in aqueous solution (135 µL) was added to the reduced R3VQ-SH **3** (1.5 mL, 2 mg/mL in PBS/NaCl) and the solution was stirred at 4 °C for 3 h at pH 6.8. The solution was then diafiltered using VIVASPIN 2000 centrifugal filter device (3,000 MWCO PES) (Sartorius). 1 mL of **5** (2.36 mg/mL) was obtained with a yield of 70%. The same reaction was also performed directly in the affinity column elution buffer (PBS/NaCl/imidazole), and gave an 83% overall yield.

AAA: Ala 14.9 (16), Arg 10.2 (10), Asp+Asn 12.2 (13), Glu+Gln 11.1 (11), Gly 24.6 (23), His* (7), Ile 3.1 (3), Leu 8.5 (8), Lys 11.7* (5), Phe 4 (4), Pro 4.8 (4), Ser 14.9 (18), Thr 9.1 (10), Tyr 5.0 (5), Val 12.6 (12). [*His cannot be determined due to co-elution with ammonium. Lys is overestimated due to co-elution with the maleimido derivative in the conditions of the analysis.]

MS: 18,113.7383 ($C_{753}H_{1168}N_{235}O_{248}S_5Gd_3$ calcd 18,113.0720).

Evaluation of the MRI properties of the contrast agents

Briefly, longitudinal and transversal relaxivities (r1 and r2) of the contrast agents as well as of a commercial solution of Gd (DOTA/Gd, DOTAREM, Guerbet, France) were assessed at 1.4 Tesla (MINISPEC mq60, Bruker, Billerica, MA), 7 Tesla (Agilent, USA) and 11.7 Tesla (Bruker, Germany). The r1 and r2 were determined from linear fits of R1 (*i.e.,* 1/T1) and R2 (*i.e.,* 1/T2) as a function of contrast agent concentration obtained by serial dilution of a stock solution in deionized water (in triplicate, from 0 to 5 mM of Gd for DOTAREM and **4**, and from 0 to 1 mM of Gd for **5**) by using the following equations:

$$(1/T1)\mathrm{obs} = (1/T1)\mathrm{d} + \mathrm{r1}[\mathrm{M}] \quad [1]$$

$$(1/T2)\mathrm{obs} = (1/T2)\mathrm{d} + \mathrm{r2}[\mathrm{M}] \quad [2]$$

where $(1/T1)\mathrm{obs}$ and $(1/T2)\mathrm{obs}$ are the observed relaxation rate, $(1/T1)\mathrm{d}$ and $(1/T2)\mathrm{d}$ are the water proton relaxation rate of the pure water solvent, and [M] is the total concentration of the contrast agent, respectively.

Detailed description of the used parameters is available in Supporting Information.

Animals and brain tissue

Brain tissues were obtained from female double transgenic PS2APP mice (overexpressing mutant forms of human presenilin 2 and human β-amyloid precursor protein, Tg(Thy1-APPSwe)71Jgr x Tg(Prnp-PSEN2*N141I)30Jgr, see also http://www.alzforum.org/research-models/ps2app-ps2n141i-x-appswe, n=10),[48] and their wild-type littermates (n=5). For the *in vitro* experiments, mice aged 18-19 months were deeply anesthetized (sodium pentobarbital, 100 mg/kg), and transcardially perfused with 0.1 M PBS pH 7.4 followed by 4% buffered paraformaldehyde (Sigma Aldrich, Germany). After perfusion, brains were

extracted, post-fixed overnight in the same fixative at 4 °C and preserved in PBS/NaCl buffer containing 0.2% of sodium azide until MRI or IHC procedures. For the *in vivo* experiments, 13-14 months PS2APP mice were injected in the tail vein with R3VQ-S-$(DOTA/Gd)_3$ at a dose of 50 mg/kg (n=3) or with PBS (n=2). Mice were sacrificed after 4 hours and IHC was performed on brain sections as described below. All animal experiments were conducted in accordance with the European Communities Council Directive (2010/63/UE). Animal care was in accordance with institutional guidelines and experimental procedures were approved by local ethics committees (authorizations 12-062; ethic committee CETEA-CEA DSV IdF).

***In vitro* procedure for MRI acquisition**

The ability of **5** to detect amyloid deposits by MRI was tested with an *in vitro* procedure on *post mortem* brains from PS2APP male mice and their wild-type littermate (PS2APP incubated with **5**: n=3; PS2APP incubated with PBS + Triton (control): n=2; wild-type incubated with **5**: n=2).

Hemispheres were incubated with **5** (300 µL at 5 mg/mL in PBS + 0.2% Triton) or PBS + 0.2% Triton overnight, followed by several wash-out cycles for at least 48 hours before MR images acquisition. These hemispheres were all imaged on an 11.7 Tesla (Bruker, Germany) spectrometer interfaced with a console running PARAVISION 6 and equipped with a rodent gradient insert of 760 mT/m used for emission, and a cryoprobe (Bruker, Germany) was used for reception. Images were acquired with a 3D-FLASH sequence (TR=40 msec, TE=15 msec, Nex=4, bandwidth=37.5 kHz, FOV=12.8x12.8x6.4 mm^3, Mtx=512x512x256, resulting in a 25 µm isotropic resolution). Hypointense spots quantification is described in the supplementary detailed experimental procedures.

Brains were then processed for 4G8 and anti-His-tag IHC as previously described.[47] MR images and histological sections were manually registered using ImageJ freeware (http://rsbweb.nih.gov/ij/): the MR images were rotated in 3 directions until the best matching planes with the histology sections were found.[73]

ACKNOWLEDGEMENTS

We are grateful to F. Bonhomme for the MS analyses by direct infusion, to F. Groh for the Amino Acid Analysis, to H. Cahuzac for helping in the synthesis of VHH conjugates, and to A. Louie (UC Davis) for providing access to 1.4 Tesla spectrometer and for training and advice on relaxometric analyses. We gratefully acknowledge financial support from the Institut Roche de Recherche et Médecine Translationnelle. This work was also supported by the program "Investissements d'avenir" ANR-10-IAIHU-06, the Pompidou Foundation and the France Alzheimer Foundation that are acknowledged. This work was partly carried out on the HISTOMICS platform of the ICM and the MRI platform of CEA-MIRCen, and we thank all technical staff involved.

REFERENCES

1. Hermanson GT. In: Bioconjugate Techniques. Antibody modification and conjugation. Academic Press; 2013. p. 783-823.
2. Beck A, Goetsch L, Dumontet C, Corvaia N. Strategies and challenges for the next generation of antibody drug conjugates. Nat Rev Drug Discov 2017; 16:315-37.
3. Behrens CR, Liu B. Methods for site-specific drug conjugation to antibodies. mAbs 2014; 6:46-53.
4. Krall N, da Cruz FP, Boutureira O, Bernardes GJL. Site-selective protein-modification chemistry for basic biology and drug development. Nature Chem 2016; 8:103-13.
5. Massa S, Xavier C, Muyldermans S, Devoogdt N. Emerging site-specific bioconjugation strategies for radioimmunotracer development. Expert Opin Drug Deliv 2016; 13:1149-63.
6. Panowski S, Bhakta S, Raab H, Polakis P, Junutula JR. Site-specific antibody drug conjugates for cancer therapy. mAbs 2014; 6:34-45.
7. Spicer CD, Davis BG. Selective chemical protein modification. Nat Commun 2014; 5:4740.
8. Kim CH, Axup JY, Schultz PG. Protein conjugation with genetically encoded unnatural amino acids. Curr Opin Chem Biol 2013; 17:412-9.
9. Tian F, Lu Y, Manibusan A, Sellers A, Tran H, Sun Y, Phuong T, Barnett R, Hehli B, Song F et al. A general approach to site-specific antibody drug conjugates. Proc Natl Acad Sci U S A 2014; 111:1766-71.
10. Junutula JR, Raab H, Clark S, Bhakta S, Leipold DD, Weir S, Chen Y, Simpson M, Tsai SP, Dennis MS et al. Site-specific conjugation of a cytotoxic drug to an antibody improves the therapeutic index. Nat Biotechnol 2008; 26:925-32.
11. Albrecht H, Burke PA, Natarajan A, Xiong CY, Kalicinsky M, DeNardo GL, DeNardo SJ. Production of soluble ScFvs with C-terminal-free thiol for site-specific conjugation or stable dimeric ScFvs on demand. Bioconjugate Chem 2004; 15:16-26.
12. Olafsen T, Cheung CW, Yazaki PJ, Li L, Sundaresan G, Gambhir SS, Sherman MA, Williams LE, Shively JE, Raubitschek AA et al. Covalent disulfide-linked anti-CEA diabody allows site-specific conjugation and radiolabeling for tumor targeting applications. Protein Eng Des Sel 2004; 17:21-7.
13. Mume E, Orlova A, Larsson B, Nilsson AS, Nilsson FY, Sjoberg S, Tolmachev V. Evaluation of ((4-hydroxyphenyl)ethyl)maleimide for site-specific radiobromination of anti-HER2 affibody. Bioconjugate Chem 2005; 16:1547-55.
14. Ahlgren S, Orlova A, Rosik D, Sandstrom M, Sjoberg A, Baastrup B, Widmark O, Fant G, Feldwisch J, Tolmachev V. Evaluation of maleimide derivative of DOTA for site-specific labeling of recombinant affibody molecules. Bioconjugate Chem 2008; 19:235-43.

15. Lundberg E, Hoiden-Guthenberg I, Larsson B, Uhlen M, Graslund T. Site-specifically conjugated anti-HER2 Affibody molecules as one-step reagents for target expression analyses on cells and xenograft samples. J Immunol Methods 2007; 319:53-63.
16. Sirk SJ, Olafsen T, Barat B, Bauer KB, Wu AM. Site-specific, thiol-mediated conjugation of fluorescent probes to cysteine-modified diabodies targeting CD20 or HER2. Bioconjugate Chem 2008; 19:2527-34.
17. Massa S, Xavier C, De Vos J, Caveliers V, Lahoutte T, Muyldermans S, Devoogdt N. Site-specific labeling of cysteine-tagged camelid single-domain antibody-fragments for use in molecular imaging. Bioconjugate Chem 2014; 25:979-88.
18. Hamers-Casterman C, Atarhouch T, Muyldermans S, Robinson G, Hamers C, Songa EB, Bendahman N, Hamers R. Naturally occurring antibodies devoid of light chains. Nature 1993; 363:446-8.
19. De Vos J, Devoogdt N, Lahoutte T, Muyldermans S. Camelid single-domain antibody-fragment engineering for (pre)clinical in vivo molecular imaging applications: adjusting the bullet to its target. Expert Opin Biol Ther 2013; 13:1149-60.
20. Harmsen MM, De Haard HJ. Properties, production, and applications of camelid single-domain antibody fragments. Appl Microbiol Biotechnol 2007; 77:13-22.
21. De Genst E, Silence K, Decanniere K, Conrath K, Loris R, Kinne R, Muyldermans S, Wyns L. Molecular basis for the preferential cleft recognition by dromedary heavy-chain antibodies. Proc Natl Acad Sci U S A 2006; 103:4586-91.
22. Lafaye P, Achour I, England P, Duyckaerts C, Rougeon F. Single-domain antibodies recognize selectively small oligomeric forms of amyloid beta, prevent Abeta-induced neurotoxicity and inhibit fibril formation. Mol Immunol 2009; 46:695-704.
23. Perruchini C, Pecorari F, Bourgeois JP, Duyckaerts C, Rougeon F, Lafaye P. Llama VHH antibody fragments against GFAP: better diffusion in fixed tissues than classical monoclonal antibodies. Acta Neuropathol 2009; 118:685-95.
24. Li Z, Krippendorff BF, Sharma S, Walz AC, Lave T, Shah DK. Influence of molecular size on tissue distribution of antibody fragments. mAbs 2015:1-7.
25. Baral TN, Magez S, Stijlemans B, Conrath K, Vanhollebeke B, Pays E, Muyldermans S, De Baetselier P. Experimental therapy of African trypanosomiasis with a nanobody-conjugated human trypanolytic factor. Nat Med 2006; 12:580-4.
26. Achour I, Cavelier P, Tichit M, Bouchier C, Lafaye P, Rougeon F. Tetrameric and homodimeric camelid IgGs originate from the same IgH locus. J Immunol 2008; 181:2001-9.

27. Vincke C, Loris R, Saerens D, Martinez-Rodriguez S, Muyldermans S, Conrath K. General strategy to humanize a camelid single-domain antibody and identification of a universal humanized nanobody scaffold. J Biol Chem 2009; 284:3273-84.
28. David MA, Jones DR, Tayebi M. Potential candidate camelid antibodies for the treatment of protein-misfolding diseases. J Neuroimmunol 2014; 272:76-85.
29. Li T, Bourgeois JP, Celli S, Glacial F, Le Sourd AM, Mecheri S, Weksler B, Romero I, Couraud PO, Rougeon F et al. Cell-penetrating anti-GFAP VHH and corresponding fluorescent fusion protein VHH-GFP spontaneously cross the blood-brain barrier and specifically recognize astrocytes: application to brain imaging. FASEB J 2012; 26:3969-79.
30. Nabuurs RJ, Rutgers KS, Welling MM, Metaxas A, de Backer ME, Rotman M, Bacskai BJ, van Buchem MA, van der Maarel SM, van der Weerd L. In vivo detection of amyloid-beta deposits using heavy chain antibody fragments in a transgenic mouse model for Alzheimer's disease. PLoS One 2012; 7:e38284.
31. Rutgers KS, Nabuurs RJ, van den Berg SA, Schenk GJ, Rotman M, Verrips CT, van Duinen SG, Maat-Schieman ML, van Buchem MA, de Boer AG et al. Transmigration of beta amyloid specific heavy chain antibody fragments across the in vitro blood-brain barrier. Neuroscience 2011; 190:37-42.
32. Rissiek B, Koch-Nolte F, Magnus T. Nanobodies as modulators of inflammation: potential applications for acute brain injury. Front Cell Neurosci 2014; 8:344.
33. Klunk WE, Engler H, Nordberg A, Wang Y, Blomqvist G, Holt DP, Bergstrom M, Savitcheva I, Huang GF, Estrada S et al. Imaging brain amyloid in Alzheimer's disease with Pittsburgh Compound-B. Ann Neurol 2004; 55:306-19.
34. Clark CM, Schneider JA, Bedell BJ, Beach TG, Bilker WB, Mintun MA, Pontecorvo MJ, Hefti F, Carpenter AP, Flitter ML et al. Use of florbetapir-PET for imaging beta-amyloid pathology. JAMA, J Am Med Assoc 2011; 305:275-83.
35. Villemagne VL, Furumoto S, Fodero-Tavoletti MT, Mulligan RS, Hodges J, Harada R, Yates P, Piguet O, Pejoska S, Dore V et al. In vivo evaluation of a novel tau imaging tracer for Alzheimer's disease. Eur J Nucl Med Mol Imag 2014; 41:816-26.
36. Maruyama M, Shimada H, Suhara T, Shinotoh H, Ji B, Maeda J, Zhang MR, Trojanowski JQ, Lee VM, Ono M et al. Imaging of tau pathology in a tauopathy mouse model and in Alzheimer patients compared to normal controls. Neuron 2013; 79:1094-108.
37. Hickey JL, Lim S, Hayne DJ, Paterson BM, White JM, Villemagne VL, Roselt P, Binns D, Cullinane C, Jeffery CM et al. Diagnostic imaging agents for Alzheimer's disease: copper radiopharmaceuticals that target Abeta plaques. J Am Chem Soc 2013; 135:16120-32.

38. Ono M, Saji H. Recent advances in molecular imaging probes for beta-amyloid plaques. MedChemComm 2015; 6:391-402.
39. Teipel S, Drzezga A, Grothe MJ, Barthel H, Chetelat G, Schuff N, Skudlarski P, Cavedo E, Frisoni GB, Hoffmann W et al. Multimodal imaging in Alzheimer's disease: validity and usefulness for early detection. Lancet Neurol 2015; 14:1037-53.
40. Santin MD, Debeir T, Bridal SL, Rooney T, Dhenain M. Fast in vivo imaging of amyloid plaques using mu-MRI Gd-staining combined with ultrasound-induced blood-brain barrier opening. NeuroImage 2013; 79:288-94.
41. Ramakrishnan M, Wengenack TM, Kandimalla KK, Curran GL, Gilles EJ, Ramirez-Alvarado M, Lin J, Garwood M, Jack CR, Jr., Poduslo JF. Selective contrast enhancement of individual Alzheimer's disease amyloid plaques using a polyamine and Gd-DOTA conjugated antibody fragment against fibrillar Abeta42 for magnetic resonance molecular imaging. Pharm Res 2008; 25:1861-72.
42. Sigurdsson EM, Wadghiri YZ, Mosconi L, Blind JA, Knudsen E, Asuni A, Scholtzova H, Tsui WH, Li Y, Sadowski M et al. A non-toxic ligand for voxel-based MRI analysis of plaques in AD transgenic mice. Neurobiol Aging 2008; 29:836-47.
43. Wadghiri YZ, Sigurdsson EM, Sadowski M, Elliott JI, Li Y, Scholtzova H, Tang CY, Aguinaldo G, Pappolla M, Duff K et al. Detection of Alzheimer's amyloid in transgenic mice using magnetic resonance microimaging. Magn Reson Med 2003; 50:293-302.
44. Yang J, Wadghiri YZ, Hoang DM, Tsui W, Sun Y, Chung E, Li Y, Wang A, de Leon M, Wisniewski T. Detection of amyloid plaques targeted by USPIO-Abeta1-42 in Alzheimer's disease transgenic mice using magnetic resonance microimaging. NeuroImage 2011; 55:1600-9.
45. Roher AE, Lowenson JD, Clarke S, Woods AS, Cotter RJ, Gowing E, Ball MJ. beta-Amyloid-(1-42) is a major component of cerebrovascular amyloid deposits: implications for the pathology of Alzheimer disease. Proc Natl Acad Sci U S A 1993; 90:10836-40.
46. Selkoe DJ. The molecular pathology of Alzheimer's disease. Neuron 1991; 6:487-98.
47. Li T, Vandesquille M, Koukouli F, Dudeffant C, Youssef I, Lenormand P, Ganneau C, Maskos U, Czech C, Grueninger F et al. Camelid single-domain antibodies: A versatile tool for in vivo imaging of extracellular and intracellular brain targets. J Control Release 2016; 243:1-10.
48. Richards JG, Higgins GA, Ouagazzal AM, Ozmen L, Kew JN, Bohrmann B, Malherbe P, Brockhaus M, Loetscher H, Czech C et al. PS2APP transgenic mice, coexpressing hPS2mut and hAPPswe, show age-related cognitive deficits associated with discrete brain amyloid deposition and inflammation. J Neurosci 2003; 23:8989-9003.

49. Cuatrecasas P, Parikh I. Adsorbents for affinity chromatography. Use of N-hydroxysuccinimide esters of agarose. Biochemistry 1972; 11:2291-9.
50. Dumoulin M, Conrath K, Van Meirhaeghe A, Meersman F, Heremans K, Frenken LGJ, Muyldermans S, Wyns L, Matagne A. Single-domain antibody fragments with high conformational stability. Protein Sci 2002; 11:500-15.
51. Olichon A, Schweizer D, Muyldermans S, de Marco A. Heating as a rapid purification method for recovering correctly-folded thermotolerant VH and VHH domains. BMC Biotechnol 2007; 7:7.
52. Papini A, Rudolph S, Siglmuller G, Musiol HJ, Gohring W, Moroder L. Alkylation of histidine with maleimido-compounds. Int J Pept Protein Res 1992; 39:348-55.
53. Paulech J, Solis N, Cordwell SJ. Characterization of reaction conditions providing rapid and specific cysteine alkylation for peptide-based mass spectrometry. Biochim Biophys Acta 2013; 1834:372-9.
54. Selkoe DJ. Toward a comprehensive theory for Alzheimer's disease. Hypothesis: Alzheimer's disease is caused by the cerebral accumulation and cytotoxicity of amyloid beta-protein. Ann N Y Acad Sci 2000; 924:17-25.
55. Caravan P, Ellison JJ, McMurry TJ, Lauffer RB. Gadolinium(III) chelates as MRI contrast agents: Structure, dynamics, and applications. Chem Rev 1999; 99:2293-352.
56. Debie P, Van Quathem J, Hansen I, Bala G, Massa S, Devoogdt N, Xavier C, Hernot S. Effect of Dye and Conjugation Chemistry on the Biodistribution Profile of Near-Infrared-Labeled Nanobodies as Tracers for Image-Guided Surgery. Mol Pharm 2017; 14:1145-53.
57. Berzofsky JA, Berkover IJ. In: Fundamental Immunology. Antigen-antibody interaction. Raven Press; 1984. p. 595-644.
58. Beck A, Wagner-Rousset E, Ayoub D, Van Dorsselaer A, Sanglier-Cianferani S. Characterization of therapeutic antibodies and related products. Anal Chem 2013; 85:715-36.
59. Wakankar A, Chen Y, Gokarn Y, Jacobson FS. Analytical methods for physicochemical characterization of antibody drug conjugates. mAbs 2011; 3:161-72.
60. Gronwall C, Sjoberg A, Ramstrom M, Hoiden-Guthenberg I, Hober S, Jonasson P, Stahl S. Affibody-mediated transferrin depletion for proteomics applications. Biotechnol J 2007; 2:1389-98.
61. Habicht G, Haupt C, Friedrich RP, Hortschansky P, Sachse C, Meinhardt J, Wieligmann K, Gellermann GP, Brodhun M, Gotz J et al. Directed selection of a conformational antibody domain that prevents mature amyloid fibril formation by stabilizing Abeta protofibrils. Proc Natl Acad Sci U S A 2007; 104:19232-7.
62. Luheshi LM, Hoyer W, de Barros TP, van Dijk Hard I, Brorsson AC, Macao B, Persson C, Crowther DC, Lomas DA, Stahl S et al. Sequestration of the Abeta peptide prevents toxicity and promotes degradation in vivo. PLoS Biol 2010; 8:e1000334.

63. Morgado I, Wieligmann K, Bereza M, Ronicke R, Meinhardt K, Annamalai K, Baumann M, Wacker J, Hortschansky P, Malesevic M et al. Molecular basis of beta-amyloid oligomer recognition with a conformational antibody fragment. Proc Natl Acad Sci U S A 2012; 109:12503-8.
64. Pain C, Dumont J, Dumoulin M. Camelid single-domain antibody fragments: Uses and prospects to investigate protein misfolding and aggregation, and to treat diseases associated with these phenomena. Biochimie 2015; 111:82-106.
65. Rotman M, Welling MM, van den Boogaard ML, Moursel LG, van der Graaf LM, van Buchem MA, van der Maarel SM, van der Weerd L. Fusion of hIgG1-Fc to 111In-anti-amyloid single domain antibody fragment VHH-pa2H prolongs blood residential time in APP/PS1 mice but does not increase brain uptake. Nucl Med Biol 2015; 42:695-702.
66. Petiet A, Delatour B, Dhenain M. Models of neurodegenerative disease - Alzheimer's anatomical and amyloid plaque imaging. Methods Mol Biol 2011; 771:293-308.
67. Jack CR, Jr., Wengenack TM, Reyes DA, Garwood M, Curran GL, Borowski BJ, Lin J, Preboske GM, Holasek SS, Adriany G et al. In vivo magnetic resonance microimaging of individual amyloid plaques in Alzheimer's transgenic mice. J Neurosci 2005; 25:10041-8.
68. Nabuurs RJ, Natte R, de Ronde FM, Hegeman-Kleinn I, Dijkstra J, van Duinen SG, Webb AG, Rozemuller AJ, van Buchem MA, van der Weerd L. MR microscopy of human amyloid-beta deposits: characterization of parenchymal amyloid, diffuse plaques, and vascular amyloid. J Alzheimers Dis 2013; 34:1037-49.
69. Amet S, Launay-Vacher V, Clement O, Frances C, Tricotel A, Stengel B, Gauvrit JY, Grenier N, Reinhardt G, Janus N et al. Incidence of Nephrogenic Systemic Fibrosis in Patients Undergoing Dialysis After Contrast-Enhanced Magnetic Resonance Imaging With Gadolinium-Based Contrast Agents The Prospective Fibrose Nephrogenique Systemique Study. Invest Radiol 2014; 49:109-15.
70. European Medicines Agency. Assessment report for Gadolinium-containing contrast agents. 2010; EMA/740640/2010.
71. Guerbet LLC. Dotarem® (gadoterate meglumine) injection. Medical Imaging Drugs Advisory Committee (MIDAC) - Advisory Committee Briefing Document NDA 204-781. U.S. Food and Drug Administration; 2013.
72. Saake M, Langner S, Schwenke C, Weibart M, Jansen O, Hosten N, Doerfler A. MRI in multiple sclerosis: an intra-individual, randomized and multicentric comparison of gadobutrol with gadoterate meglumine at 3 T. Eur Radiol 2016; 26:820-8.
73. Petiet A, Santin M, Bertrand A, Wiggins CJ, Petit F, Houitte D, Hantraye P, Benavides J, Debeir T, Rooney T et al. Gadolinium-staining reveals amyloid plaques in the brain of Alzheimer's transgenic mice. Neurobiol Aging 2012; 33:1533-44.

Table 1: ELISA evaluation of antigen binding properties against Aβ40 for R3VQ-NH_2 **1**, R3VQ-SH **3** and their respective conjugates **2a**, **2b**, and **5**, highlighting the intact antigen recognition for the site-specific conjugate.

Compound	**IC_{50} (nM)[a]**
1	16
2a	24
2b	50
3	18
5	19

[a]IC_{50} values were determined by measuring the amount of soluble Aβ40 peptide able to give 50% inhibition of VHH binding to immobilized Aβ40.

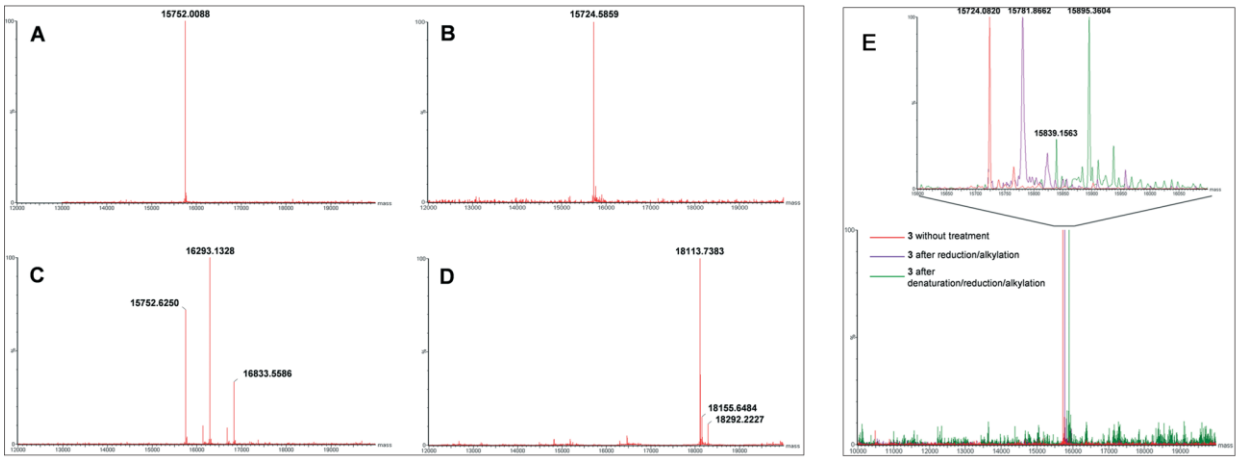

Figure 1: MS analyses of compounds involved in random (A, C) and site-specific approaches (B, D). Analyses (deconvoluted spectra) of starting VHHs **1** (expected M_r=15,752.3949) (A) and **3** (expected M_r=15,724.2820) (B), and their respective DOTA/Gd conjugates **2a** (expected M_r=16,293.0421 $(DOTA/Gd)_1$, 16,833.6735 $(DOTA/Gd)_2$) (C) and **5** (expected M_r=18,113.0720) (D) showed the polydisperse mixture obtained with **2a** as opposed to the well-defined conjugate **5**.

MS analyses of R3VQ-SH **3** showing the presence of a single reduced cysteine and of a stable disulfide bond (E). Analyses (deconvoluted spectra) were realized on **3** without treatment (expected M_r=15,724.2820), after reduction/alkylation (expected M_r=15,781.3339 with 1 alkylated cysteine), and after denaturation/reduction/alkylation experiments (expected M_r=15,895.4378 with 3 alkylated cysteines). The magnified overlay (top) showed the shifts due to alkylation of the thiol functions depending on conditions.

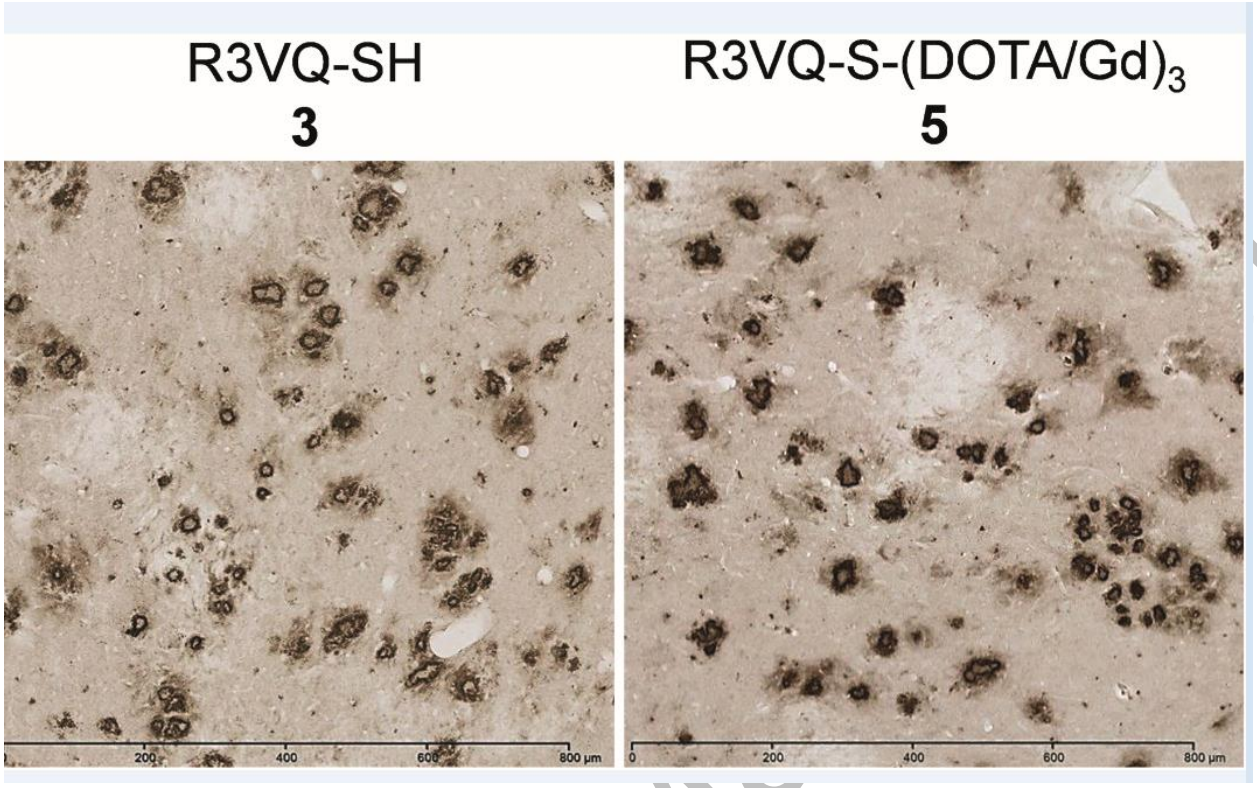

Figure 2: Immunostaining of amyloid deposits by R3VQ-SH **3** (left) and R3VQ-S-(DOTA/Gd)$_3$ **5** (right) on brain tissue from mouse model of amyloidosis, showing the preserved properties of the site-specific conjugate (see Figure S7 for IHC controls).

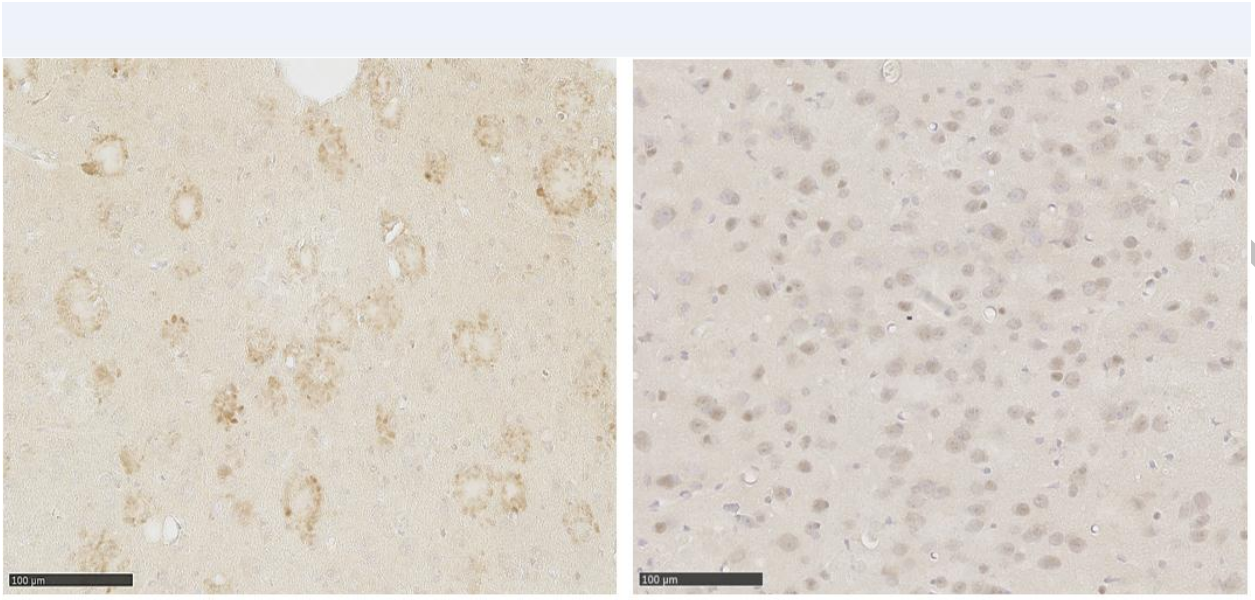

Figure 3: Immunostaining of amyloid plaques after intravenous injection of R3VQ-S-$(DOTA/Gd)_3$ **5**, highlighting its ability to cross the BBB *in vivo*.

PS2APP mice (15 month-old) were injected in the tail vein with compound **5** at 50 mg/kg (left panel, n=3) or with PBS (right panel, n=2), and sacrificed after 4 hours. IHC were realized with an anti-His-tag antibody. Whereas only unspecific background was observed in mice brains injected with PBS, a specific labeling of amyloid deposits was detected in those injected with **5** thus confirming the ability of the conjugate to cross the BBB after *in vivo* injection.

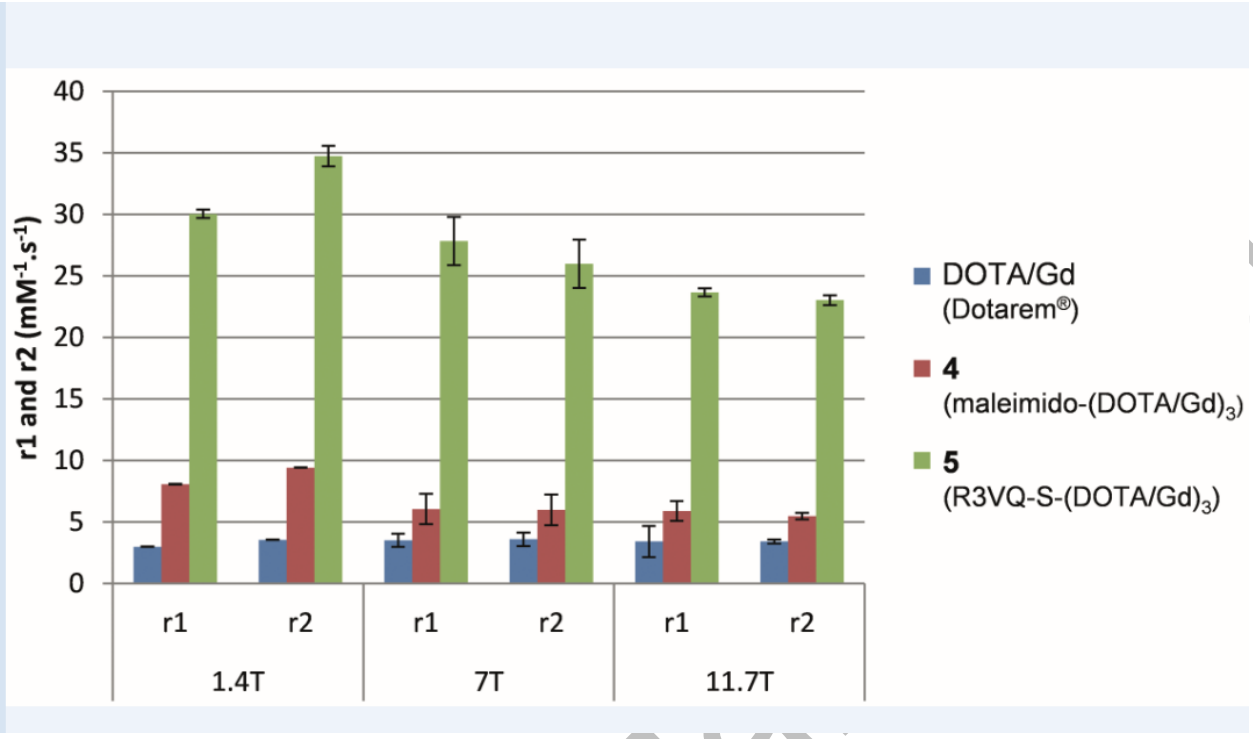

Figure 4: MR relaxometric parameters at three different magnetic fields. Measures of r1 and r2 (normalized per mM of Gd) showed the high relaxivities of the contrast agent R3VQ-S-$(DOTA/Gd)_3$ **5** that reach values until 10 times higher than those of the reference contrast agent DOTAREM. Triplicate measures of r1 and r2 (in $mM^{-1}.s^{-1}$) are expressed as mean +/- SEM (detailed values in Figure S9).

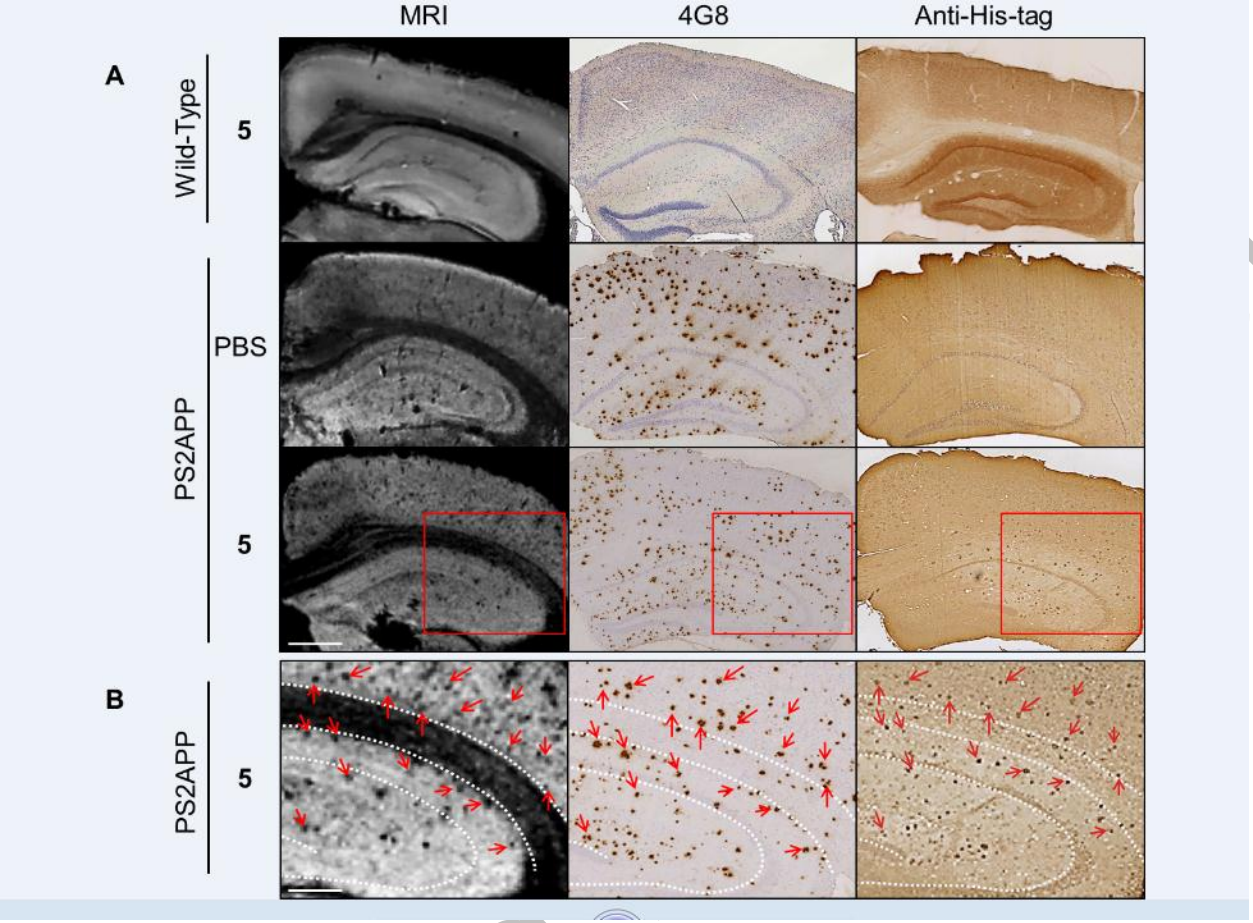

Figure 5: *In vitro* MRI revelation of amyloid deposits by the contrast agent R3VQ-S-(DOTA/Gd)$_3$ **5**.
A. PS2APP or wild-type (amyloid free) brains were incubated with PBS or **5** before MRI acquisitions (left frames). IHC were realized with 4G8 antibody as a reference anti-beta amyloid antibody (middle frames), or an anti-His-tag antibody to reveal the amyloid deposits labeled by the contrast agent **5** (right frames). MRI acquisitions were performed with a 25 µm isotropic resolution (n=2/group). Red squares show the magnified areas used for the registration. Scale bar = 500 µm. See Figure 6 for hypointense spots quantification. B. Registration was done between MRI, 4G8 and anti-His-tag IHC on PS2APP tissues incubated with **5**. Hypointense spots on MR images correspond to amyloid deposits labeled by **5** on the anti-His-tag IHC and by 4G8 (red arrows). White dotted lines represent landmarks that delimited the corpus callosum and the hippocampus. Scale bar = 250 µm.

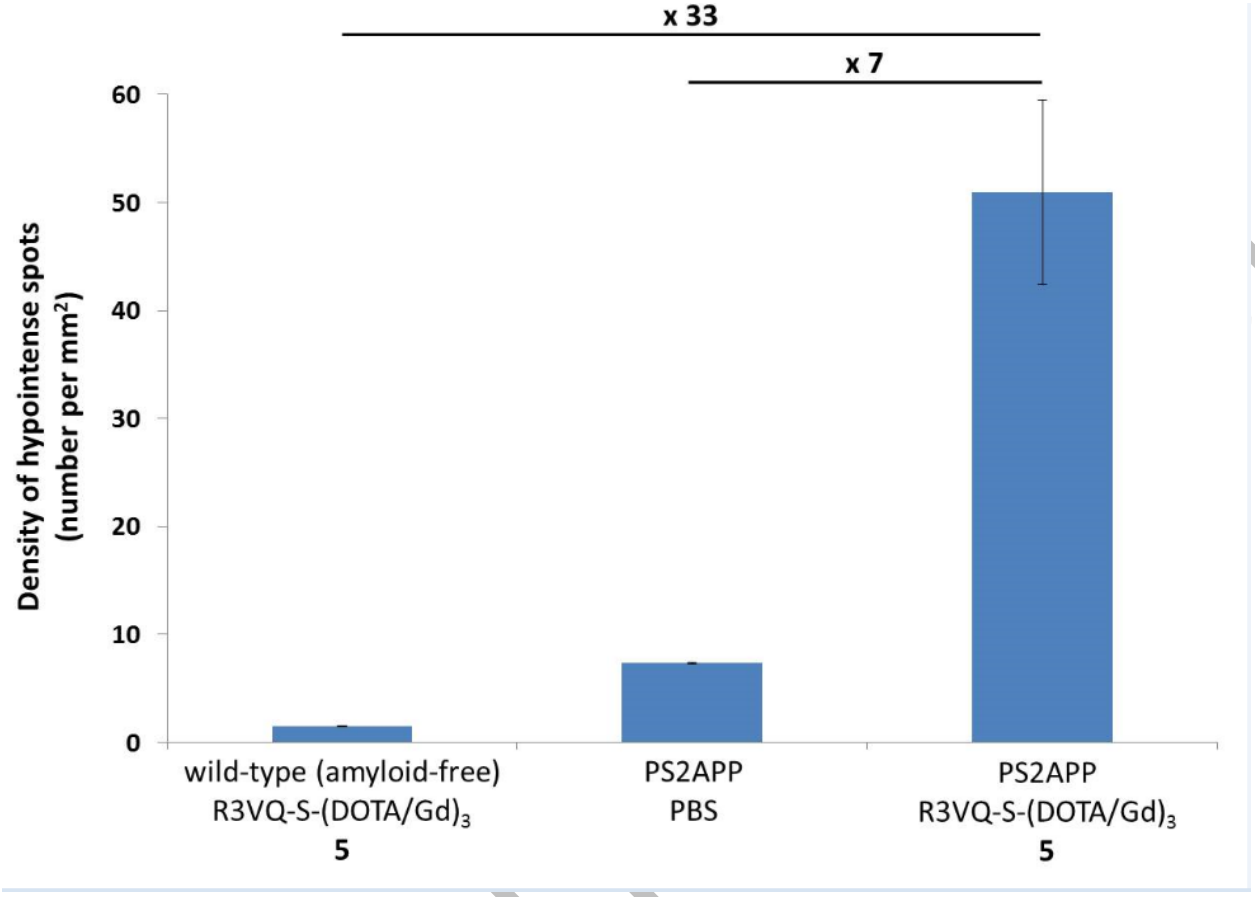

Figure 6: Quantification of hypointense spots detected on MR images.

Measures from MR images obtained on *post mortem* brain tissues (Figure 5A) confirmed the major increase in amyloid plaques detection in PS2APP brains incubated with the R3VQ-S-(DOTA/Gd)$_3$ **5** compared to the controls, *i.e.,* PS2APP brains incubated with PBS or wild-type amyloid-free brains incubated with R3VQ-S-(DOTA/Gd)$_3$ **5**.

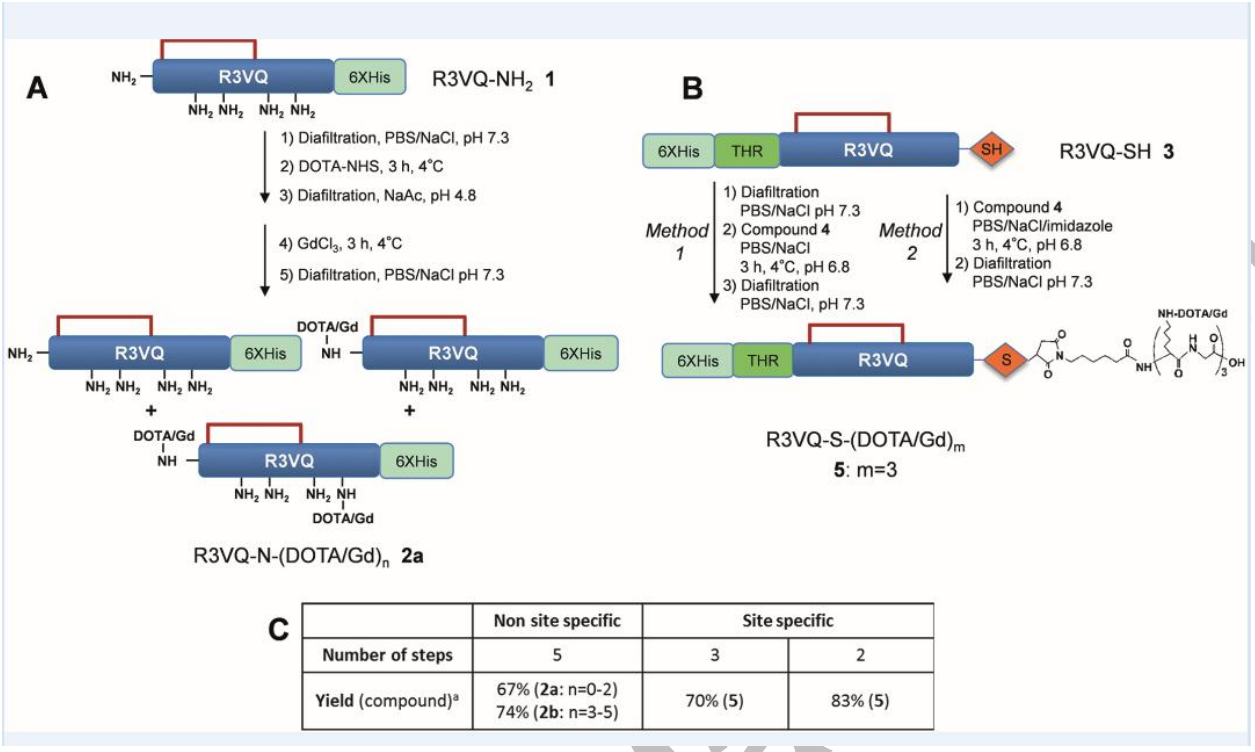

C

	Non site specific	Site specific	
Number of steps	5	3	2
Yield (compound)[a]	67% (**2a**: n=0-2) 74% (**2b**: n=3-5)	70% (**5**)	83% (**5**)

Scheme 1. Overview of random (A) and site-specific (B) chemical conjugation[a] [a]Reagents and conditions: (a) Diafiltration, PBS/NaCl, pH 7.3; (b) DOTA-NHS, 3 h , 4 °C; (c) Diafiltration, NaAc, pH 5; (d) $GdCl_3$, 3 h, 4 °C; (e) Compound **4**, PBS/NaCl, 3 h, 4 °C, pH 6.8.

The site-specific conjugation (B) was performed with (method 1) or without (method 2) initial buffer exchange. Synthesis of compound **4** is described in Scheme 2. Table C summarizes the number of steps and the overall yield of each approach (include all the synthetic process from the starting protein in the affinity column elution buffer). n = average amount of DOTA/Gd per VHH (randomly distributed on different sites). m = exact amount of DOTA/Gd per VHH (located on a single site).

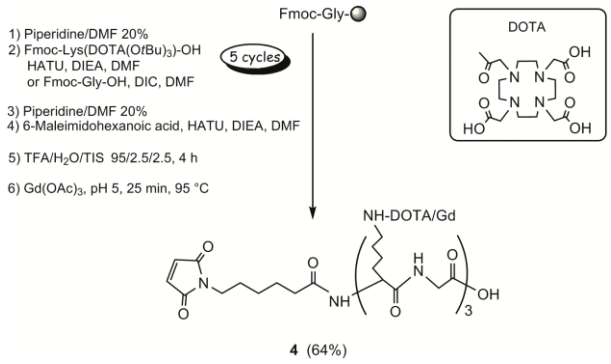

Scheme 2. Synthesis of maleimide-(DOTA/Gd)$_3$ 4[a, a] Reagents and conditions: (a) piperidine/DMF 20%; (b) Fmoc-Lys(DOTA(O*t*Bu)$_3$)-OH, HATU, DIEA, DMF or Fmoc-Gly-OH, DIC, DMF; (c) 6-Maleimidohexanoic acid, HATU, DIEA, DMF; (d) TFA/H_2O/TIS, 95/2.5/2.5, 4 h; (e) Gd(OAc)$_3$, pH 5, 25 min, 95 °C.